The Astrophysical Journal, 774:34 (9pp), 2013 September 1 doi:10.1088/0004-637X/774/1/34

FAR-ULTRAVIOLET OBSERVATIONS OF THE SPICA NEBULA AND THE INTERACTION ZONE

Yeon-Ju Choi[1], Kyoung-Wook Min[1], Kwang-Il Seon[2], Tae-Ho Lim[1], Young-Soo Jo[1], and Jae-Woo Park[3]
[1] Korea Advanced Institute of Science and Technology (KAIST), 373-1 Guseong-dong, Yuseong-gu, Daejeon 305-701, Korea; zmzm83@kaist.ac.kr
[2] Korea Astronomy and Space Science Institute (KASI), 61-1 Hwaam-dong, Yuseong-gu, Daejeon 305-348, Korea
[3] Korea Intellectual Property Office (KIPO), Government Complex Daejeon Building 4, 189 Cheongsa-ro, Seo-gu, Daejeon 305-348, Korea
Received 2013 April 15; accepted 2013 July 5; published 2013 August 13

ABSTRACT

We report the analysis results of far-ultraviolet (FUV) observations, made for a broad region around α Vir (Spica) including the interaction zone of Loop I and the Local Bubble. The whole region was optically thin and a general correlation was seen between the FUV continuum intensity and the dust extinction, except in the neighborhood of the bright central star, indicating the dust scattering nature of the FUV continuum. We performed Monte Carlo radiative transfer simulations to obtain the optical parameters related to the dust scattering as well as to the geometrical structure of the region. The albedo and asymmetry factor were found to be 0.38 ± 0.06 and 0.46 ± 0.06, respectively, in good agreement with the Milky Way dust grain models. The distance to and the thickness of the interaction zone were estimated to be 70^{+4}_{-8} pc and 40^{+8}_{-10} pc, respectively. The diffuse FUV continuum in the northern region above Spica was mostly the result of scattering of the starlight from Spica, while that in the southern region was mainly due to the background stars. The C IV λλ1548, 1551 emission was found throughout the whole region, in contrast to the Si II* λ1532 emission which was bright only within the H II region. This indicates that the C IV line arises mostly at the shell boundaries of the bubbles, with a larger portion likely from the Loop I than from the Local Bubble side, whereas the Si II* line is from the photoionized Spica Nebula.

Key words: H II regions – ISM: individual objects (Spica Nebula, Interaction Zone) – ultraviolet: ISM

Online-only material: color figures

1. INTRODUCTION

Observations in the far-ultraviolet (FUV) wavelengths (900–1750 Å) provide a wealth of information regarding the physical and chemical processes in the interstellar medium (ISM). For example, many important ion emission lines associated with the cooling hot gas of $T \sim 10^{4.5}$–$10^{5.5}$ K, such as C III λ977; O VI λλ1032, 1038; and C IV λλ1548, 1551, exist in this wavelength range (Slavin 1989; Borkowski et al. 1990; Landini & Monsignori Fossi 1990). The wavelength band also includes the fluorescence emission lines of the Lyman transitions of molecular hydrogen, which arise in the photodissociation regions (PDRs; Sternberg 1989). Furthermore, the diffuse FUV continuum background radiation probes the dust scattering of starlight (Bowyer 1991; Henry 2002; Seon et al. 2011a, 2011b). Hence, a variety of astrophysical targets have been analyzed based on FUV observations, such as supernova remnants (Seon et al. 2006; Kim et al. 2010a, 2010b), superbubbles (Kim et al. 2007; Jo et al. 2011, 2012), diffuse and molecular clouds, and interstellar dust (Lee et al. 2006; Park et al. 2009, 2012; Lim et al. 2013).

FUV observations are also useful in the study of H II regions around bright stars. One example is the Spica Nebula. Spica (α Vir), located at $(l, b) = (316.^\circ11, 50.^\circ84)$, is a spectroscopic binary system with a primary star of the B1 III–IV type and a secondary star of the B2 V type, and is at a distance of ∼80 pc from the Sun in the direction toward the Scorpius–Centaurus (Sco–Cen) association. The Spica Nebula is relatively isolated, as revealed by its Wisconsin Hα Mapper image (Haffner et al. 2003), and is characterized by a low gas density of 0.2–0.6 cm^{-3} (Reynolds 1985; Park et al. 2010). Park et al. (2010) analyzed its spectral images from the Si II* λ1533 and Al II λ1671 lines and found enhancement of the Si II* intensity in the southern region, a feature also seen in the Hα image. They attributed the feature to the density increase in the southern region. In contrast, the image of the Al II λ1671 line presented a broad central peak around the central star without significant enhancement in the southern region. The broad central peak was ascribed to the effect of multiple resonant scattering. An ambient dust cloud was also reported in the H II region from the analysis of *Infrared Astronomical Satellite* (*IRAS*) 60 μm and 100 μm observations (Zagury et al. 1998). Murthy & Henry (2011) noted the FUV halo around Spica and attributed it to dust scattering by the central star Spica. They tried to constrain the distance to the dust layers with a single scattering model. We will further discuss their results later for comparisons with our model.

The Spica Nebula is located close to the so-called the interaction zone of the Local Bubble (hereafter, LB) and the Loop I superbubble (Egger & Aschenbach 1995). The existence of the LB was inferred from soft X-ray background observations (Cox & Reynolds 1987). It is a low-density ($\sim 5.0 \times 10^{-3}$ cm^{-3}) region with a radius of ∼100 pc, inside which the solar system is embedded. A number of direct and indirect observations have revealed a cool and dense neutral hydrogen gas layer with a column density N(H I) of $\sim 1.0 \times 10^{19}$ cm^{-2} (Cox & Reynolds 1987; Lallement et al. 2003) to be an expanding boundary of the LB (Knude 1978; Ferlet et al. 1985; Fruscione et al. 1994; Welsh et al. 1994). Nevertheless, the shape, origin, and the ionization structure of the LB are still under debate (Cox 1998; Welsh et al. 2010; de Avillez & Breitschwerdt 2012). Loop I is a large radio loop centered on $(l, b) = (329^\circ \pm 1.^\circ5, 17.^\circ5 \pm 3^\circ)$ with an angular radius of ∼58°. It is believed to have been formed by multiple supernova explosions and/or strong stellar winds of the Sco–Cen OB association located ∼170 pc from the Sun. The boundary of Loop I was observed to be expanding with a velocity of ∼20 km s^{-1} into the neutral ambient medium of density $n \sim 0.6$ cm^{-3}, forming a dense neutral shell with column density N(H I) of $\sim 1.0 \times 10^{20}$ cm^{-2}

at the terminal shock (Sofue et al. 1974; Egger & Aschenbach 1995). There is a wealth of evidence that Loop I consists of a low density ($\sim 2.5 \times 10^{-3}$ cm^{-3}), hot ($\sim 10^{6.5}$ K), and highly ionized X-ray emitting gas generated by the interaction between the shock waves from the recent supernova explosions within the Sco–Cen association and the ambient neutral medium (Egger & Aschenbach 1995; Breitschwerdt et al. 2000; Willingale et al. 2003; Welsh & Lallement 2005). The X-rays, together with the young OB stars of the Sco–Cen association, are believed to provide intense radiations that are responsible for the ionization of neutral gas at the Loop I boundary, probably on the inner side of the boundary wall (Welsh & Lallement 2005).

The interaction zone is a huge ring-like feature of a dense neutral matter within the apparent boundary of the Loop I shell, as identified by Egger & Aschenbach (1995) from the analysis of diffuse X-ray and 21 cm neutral hydrogen maps. The feature has been suggested to be a colliding structure of Loop I with the LB. Yoshioka & Ikeuchi (1990) predicted the ring-like feature using hydrodynamical simulations; when a shock at the boundary of a bubble in a radiative stage makes contact with a shock of another bubble, a dense neutral wall of ring-like shape with density 20–30 times higher than those of the ambient medium would be formed at the intersecting points of the two bubbles. Egger & Aschenbach (1995) noted that the N(H I) of this region suddenly jumps from $\sim 10^{20}$ cm^{-2} to $\sim 7.0 \times 10^{20}$ cm^{-2} at a distance of $\sim$70 pc from the Sun using the absorption measurements of metal ions by Fruscione et al. (1994), and they suggested the distance to the interaction zone to be $\sim$70 pc. Assuming a toroidal shape of thickness of $\sim 12^{\circ}$, corresponding to $\sim$15 pc at 70 pc, its density was estimated to be $\sim$15 cm^{-3}. Breitschwerdt et al. (2000) set the upper limit of the distance of the interaction zone to be 80–100 pc since Loop I, being still active with ongoing star formations, may have a higher pressure than the adjacent LB and push the interaction shell toward the LB. Corradi et al. (2004), using Strömgren photometry and Na I column density measurements, estimated the distance to the interaction zone to be 120–150 pc. On the other hand, Reis & Corradi (2008) suggested that the ring-shaped interaction zone may be folded and warped as both the distance to the ring and the color excess values vary along the ring; they estimated the distance to the interaction zone to be 110 ± 20 pc on the western side and 280 ± 50 pc on the eastern side.

In this paper, we present the analysis results of the FUV observations of an extended region around the Spica Nebula that includes the interaction zone. The main goal of this study is to understand the morphological relationship between the Spica Nebula and the neighboring interaction zone as well as the scattering properties of the associated dust clouds using the FUV observations and radiative transfer models.

2. DATA

We employed two data sets for this study: one is from the archival FUV data of *Galaxy Evolution Explorer* (*GALEX*; Morrissey et al. 2007), obtained as part of the All-Sky Imaging Survey, and the other is the data set used by Park et al. (2007, 2010), obtained from the Far-ultraviolet Imaging Spectrograph (FIMS; Edelstein et al. 2006a, 2006b) on board the Korean microsatellite *STSAT-1*. Both observations cover very similar FUV wavelength bands of 1350–1780 Å and 1330–1720 Å for *GALEX* and FIMS, respectively. They are complementary to each other in that the *GALEX* data have good statistics but no spectral information, while the FIMS data provides spectral information but with rather large statistical fluctuations due to relatively short exposure time and lower sensitivity. Hence, we use the *GALEX* data for photometric analyses as it gives more reliable estimations of the diffuse FUV intensities than the FIMS data, while we use the FIMS data for spectral analyses as it can discriminate the FUV line emissions from the stellar continuum emissions. The *GALEX* sky background data (with an extension of skybg), provided with a resolution of 16′ (Morrissey et al. 2007) and taken from the Web site http://galex.stsci.edu/GR6/, were smoothed to obtain the final image with a resolution of 0.°5. The data reduction procedures of the FIMS data are described in detail by Park et al. (2007). More information on the instrument FIMS can be found in Edelstein et al. (2006a, 2006b).

3. RESULTS

Figure 1 shows the *GALEX* FUV image, together with the maps obtained from the observations made in other wavelengths. The figures are shown for an extended region of $24^{\circ} \times 24^{\circ}$ around the Spica Nebula, in which the central star α Vir is marked with an asterisk at $(l, b) = (316.°11, 50.°84)$. A black circle of 8° radius, defining the boundary of the Spica Nebula, is also drawn in each of the figures. In Figure 1(a), the missing data regions shown in black are the regions of bright stars that were intentionally avoided during the observations. The Hα map in Figure 1(b), scaled in units of rayleighs (1 R = $(10^6/4\pi)$ photons cm^{-2} sr^{-1} s^{-1}), was extracted from the Hα sky survey map of Finkbeiner (2003) and Haffner et al. (2003). The H I column density map in Figure 1(c), shown in units of 10^{20} cm^{-2}, was taken from the Leiden Argentine Bonn Galactic H I Survey (Kalberla et al. 2005). The dust extinction map in Figure 1(d) was obtained from the Galactic reddening map of Schlegel et al. (1998), which was derived from *Cosmic Background Explorer* (*COBE*) and *IRAS* observations.

First, we note that the Hα intensity is mostly confined within a finite volume of the ionized nebula and drops abruptly at the southern boundary near the interaction zone of the LB and Loop I, while the FUV intensity continues southward beyond the boundary of the nebula. Park et al. (2010) argued that the H II region is "ionization bounded" at the boundary in the southern region with N(H I) $\sim 6.0 \times 10^{20}$ cm^{-2}, below which a good correlation is seen between the H I column density and the Hα intensity. This conclusion accords well with the fact that the estimated distance to the interaction zone is $\sim$70 pc, which is comparable to that of the Spica Nebula.

There are two noticeable features in the FUV map: a halo around the central star α Vir and an extended feature that generally traces dust in the interaction zone. The FUV halo around α Vir is best seen in the northern region above the star; it is a dust-scattered feature of the α Vir starlight. The extended FUV feature in the southern region is predominant, as will be discussed in Section 3, due to scattering of starlight originating from other background stars by dust in the interaction zone.

Figure 2(a) shows a pixel-to-pixel correlation plot between the FUV intensity and the dust extinction in the whole region of $24^{\circ} \times 24^{\circ}$ except for a bright central part of angular size of 3.°5 around Spica. In the figure, the data points with $E(B-V) < 0.06$, denoted in blue, were mostly obtained in the northern region above the central star, while those with $E(B-V) > 0.06$, denoted in black, were obtained in the southern region. It should be noted that the color excess $E(B-V)$ in the whole region is less than 0.14, which corresponds to the optical depth of $\tau \sim 1$ at 1565 Å, and thus a general correlation between the FUV intensity and dust extinction is expected if the radiation field is

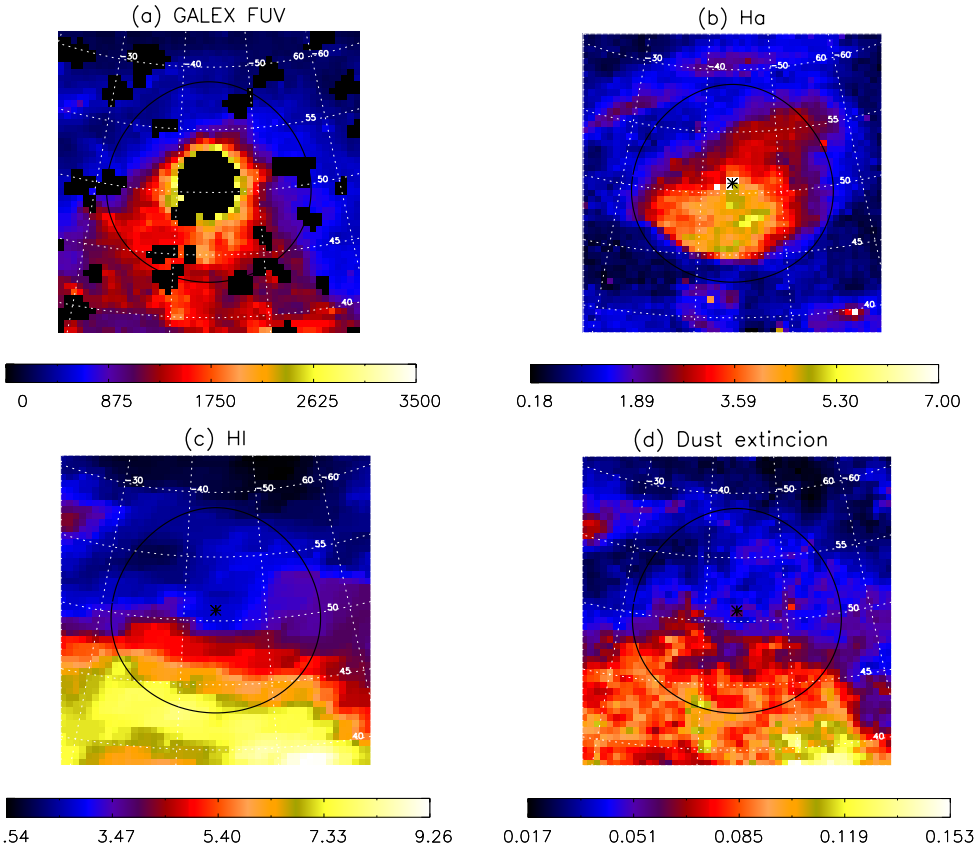

Figure 1. Extended Spica Nebula region observed in various wavelengths: (a) the *GALEX* FUV intensity in CU (photons sr^{-1} s^{-1} cm^{-2} $Å^{-1}$), (b) the Hα intensity in rayleighs (1 R = $(10^6/4\pi)$ photons cm^{-2} sr^{-1} s^{-1}), (c) the H I column density in units of 10^{20} cm^{-2}, and (d) the dust extinction given by $E(B-V)$. The images are shown in galactic coordinates. The black circles of radius 8° denote the boundary of the Spica Nebula. The central star α Vir is marked with an asterisk at $(l, b) = (316.^\circ11, 50.^\circ84)$.

(A color version of this figure is available in the online journal.)

uniform (Hurwitz 1994). The figure does show a general trend of increasing FUV intensity as $E(B-V)$ increases, except that the data points are severely scattered for the values of $E(B-V)$ from 0.04 to 0.08 while their intensities are limited to ~2000 CU. The severe scattering in the FUV intensity is clearly a distance effect as the FUV intensity depends strongly on the distance from the central star in this bright region close to Spica, while the maximum value of ~2000 CU is a result of the brighter regions being excluded from the observations. Nevertheless, excluding this large dispersion, we see an increasing dispersion of the FUV intensity with increasing $E(B-V)$. Seon et al. (2011a) & Seon (2013) noted this property in the analyses of the FUV continuum background, and attributed it to the lognormality of the FUV intensity, caused by the turbulence property of the ISM. It is well known that the probability distribution functions of the ISM density and column density are very close to lognormal (Vazquez-Semadeni 1994; Klessen 2000; Burkhart & Lazarian 2012; Seon 2012). Since the dust-scattered intensity is roughly proportional to the dust column density, the FUV intensity should exhibit a signature of the lognormal density structure. They also found that the dispersion of the FUV intensity is consistent with that observed in the turbulent molecular clouds.

It is also interesting to see that in Figure 2(b), which is an enlarged plot for the low extinction part of Figure 2(a), both the FUV intensity and the dust extinction $E(B-V)$ have minimum values of ~200 CU and ~0.015, respectively. The minimum FUV intensity of ~200 CU is comparable to the so-called isotropic component of ~300 CU (Bowyer 1991; Henry 2002; Seon et al. 2011a), although some part of it may also come from airglow (Sujatha et al. 2010). These minimum values could be regarded as background values that are not relevant to the region considered in this study.

Figure 3 shows good correlation between the neutral atomic hydrogen column density N(H I) and $E(B-V)$. The figure reveals that the ratio of N(H I) to $E(B-V)$ was ~7.0×10^{21} atoms cm^{-2} mag^{-1}. There have been several studies to estimate the ratio in the general diffuse ISM. Using 21 cm data, Knapp & Kerr (1974) and Burstein & Heiles (1978) obtained an average ratio of ~5.0×10^{21} atoms cm^{-2} mag^{-1}. Savage & Mathis (1979) used the Lyα absorption data obtained toward 100 stars by the *Copernicus* spacecraft and found a ratio of 4.8×10^{21} atoms cm^{-2} mag^{-1}. Diplas & Savage (1994a, 1994b) employed 393 sample stars observed with the *International Ultraviolet Explorer* (*IUE*) satellite and obtained 4.93×10^{21} atoms cm^{-2} mag^{-1} in the regime of $E(B-V) \leqslant 0.6$, and 5.53×10^{21} atoms cm^{-2} mag^{-1} in the lower color excess values of $E(B-V) \leqslant 0.3$. The increase in the N(H I) to $E(B-V)$ ratio in the lower color regime was attributed to the fact that a significant amount of hydrogen is in molecular form for $E(B-V) > 0.3$. The present result is higher than these previous values, implying that dust is probably less abundant in the shell boundaries of the LB and Loop I. The evaporation of dust by the hot gas of the LB and Loop I and/or the expelling of dust by the strong radiation pressure from the young OB stars of the Sco–Cen association might be responsible for this deficiency of dust.

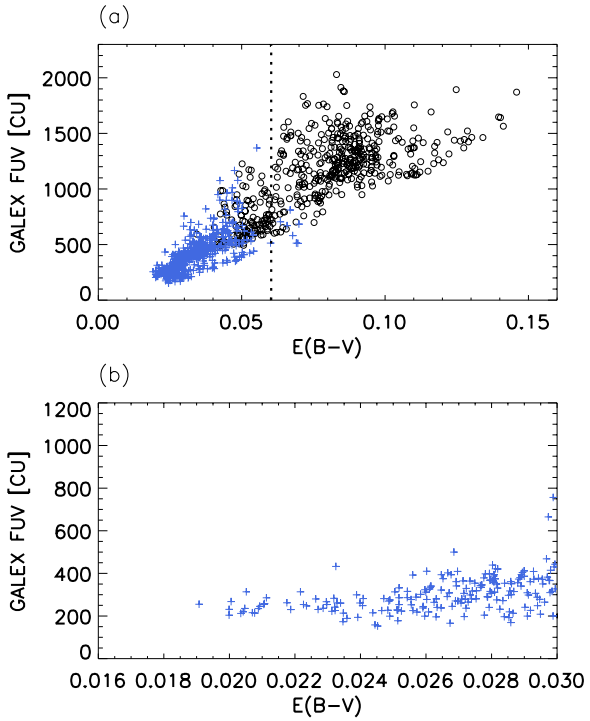

Figure 2. Correlation plots between the FUV intensity and dust color excess in the region outside the bright circular region with an angular radius of 3.°5. (a) is for the entire region and (b) is an enlarged plot for $E(B-V) < 0.03$. The data points marked with blue crosses represent the northern region above the central star α Vir and those with black circles represent the southern region below the star.

(A color version of this figure is available in the online journal.)

Figure 4(a), made by utilizing the HEALPix scheme (Górski et al. 2005) with a pixel resolution of 0.°5, was constructed from the FIMS data of the 1360–1660 Å wavelength band, excluding the airglow line of λ1356 and the Al II line of λ1671. We removed the pixels of bright background stars and filled them by interpolating the intensity from the neighboring pixels. A total of ∼50 bright pixels were removed based on the TD-1 stellar catalog (Thompson et al. 1978). The bright streak inside the narrow rectangular box is an artifact due to the instrumental scattering of the bright central star along the slit direction. The color levels are the same as those adopted for the *GALEX* image in Figure 1(a). The two images of *GALEX* and FIMS are very similar, although the FIMS intensity varied less than the *GALEX* data because of smoothing of the FIMS image. In Figure 4(b), the top panel shows the spectrum of the core region inside an angular radius of 0.°5, and the middle and bottom panels show the spectra of the diffuse emission in the two outer regions A and B, respectively. The spectrum of the top panel is dominated by the central star (α Vir), and its shape is consistent with the stellar spectrum of Spica observed by *IUE*. The Si II* and C IV ion lines are found in the outer region spectra at wavelengths ∼1533 Å and ∼1550 Å, respectively. The Si II* line was studied by Park et al. (2010) using a photo-ionization model appropriate to the Spica Nebula. The Si II* emission was mostly observed within the nebula and its intensity was slighter higher in the southern part than in the northern part. We fitted the C IV doublet lines observed in the outer region spectra using the IDL-based MPFIT (Markwardt 2009) by assuming two Gaussian functions, as done in Seon et al. (2006); the best-fit intensities are ∼5800 ± 1100 photons s^{-1} cm^{-2} sr^{-1} (line units, LU) and ∼4300 ± 1200 LU for the northern and southern

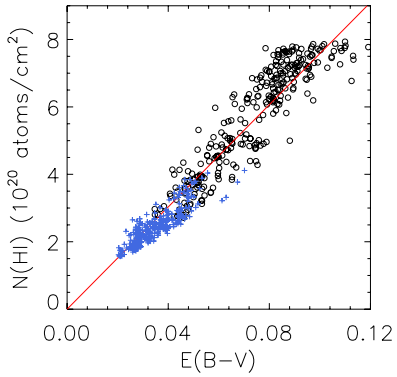

Figure 3. Pixel-to-pixel comparison of N(H I) with $E(B-V)$, as obtained from Figures 1(d) and (c). The blue crosses and the black circles are the data points obtained from the northern and the southern regions, respectively. The red line represents the best-fit ratio of N(H I) to $E(B-V)$.

(A color version of this figure is available in the online journal.)

regions, respectively. The large errors in the results are mainly due to the fact that the results were obtained from a wide region in which C IV intensity fluctuated significantly and the exposure time was rather short. We also note that the molecular hydrogen fluorescence lines are found in the spectrum of the southern region corresponding to the interaction zone.

4. MODELING AND DISCUSSION

Spica is likely located close to the interaction zone of the LB and Loop I, as mentioned in the Introduction. Since Loop I is observed to be expanding into the ambient medium of ∼0.6 cm^{-3}, the density of the ambient medium would be similar to that the Spica Nebula region. Reynolds (1985) and Park et al. (2010) estimated a density of ∼0.6 cm^{-3} and ∼0.22–0.36 cm^{-3}, respectively, implying that Spica is located in the ambient medium outside the two bubbles. It is also interesting to note that the H I column density toward Spica was estimated to be $\sim 10^{19}$ cm^{-2} (Shull & van Steenberg 1985; Fruscione et al. 1994), which is similar to the column density of the shell boundary of the LB (Cox & Reynolds 1987; Lallement et al. 2003). The shell boundary of Loop I had a column density of $\sim 10^{20}$ cm^{-2} (Sofue et al. 1974; Egger & Aschenbach 1995). These observations suggest that Spica is located behind the LB shell but in front of the Loop I shell. The density (∼15 cm^{-3}; Egger & Aschenbach 1995) of the interaction zone was much higher than that of the Spica Nebula. This indicates that Spica is located slightly away from the interaction zone. Taking all these considerations into account, the relative geometry between the LB, Loop I, and Spica could be represented by a schematic diagram shown in Figure 5.

As we discussed previously, the interaction zone is rich in dust and its column density N(H I) is proportional to the level of dust extinction, implying that dust responsible for the scattering of starlight should be located close to the central star and the interaction zone. This will be confirmed by modeling the scattered stellar photons by assuming dust distributions. A similar study was conducted by Murthy & Henry (2011) for the halo around Spica observed by *GALEX*. They focused on the region close to the star and ignored the dust scattering effect in the interaction zone. They employed a single dust-scattering model and assumed only a single star (i.e., α Vir). In their first model, they placed a thin dust sheet at a distance of 3 pc from the star, inferred from the 60 μm and 100 μm infrared observations, and obtained a very low albedo value of 0.10 ± 0.05 in the FUV

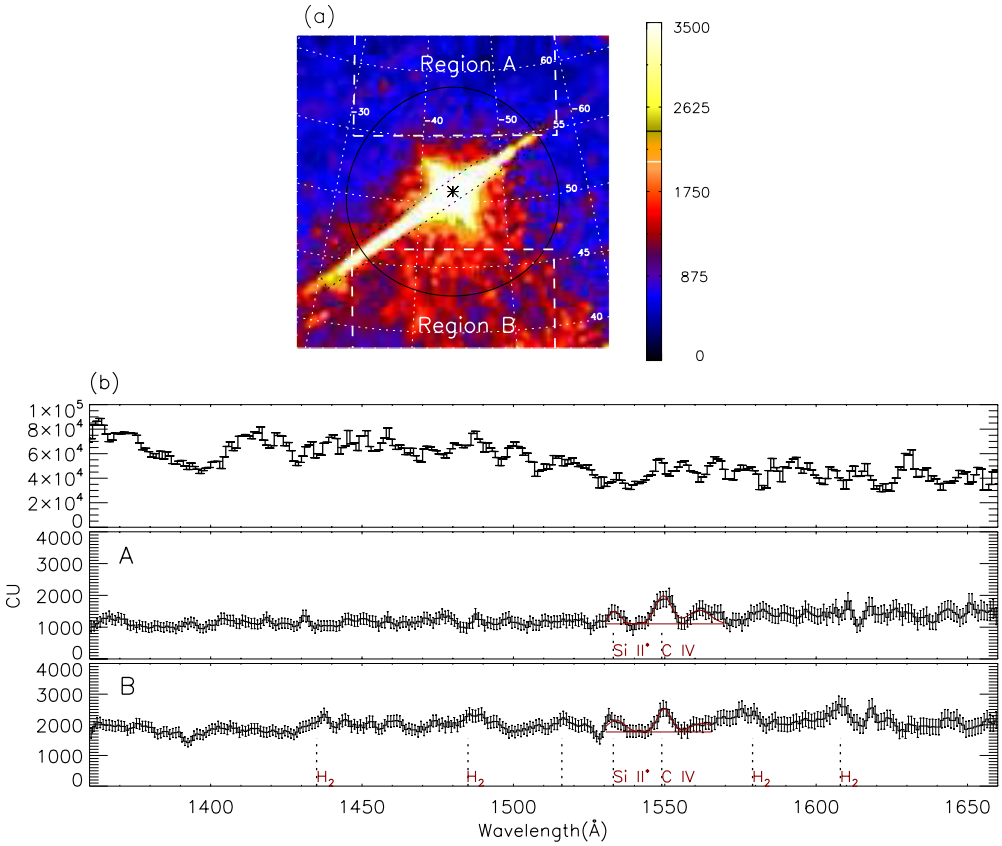

Figure 4. (a) The FUV intensity map observed by FIMS is given in CU (photons sr^{-1} s^{-1} cm^{-2} $Å^{-1}$). The bright streak in the narrow rectangular box is due to the instrumental scattering of the bright central star along the slit direction. The black circle of radius of 8° indicates the boundary defining the Spica Nebula. The central star, α Vir, is marked with an asterisk at (l, b) = (316.°11, 50.°84). (b) Spectra observed by FIMS: the top panel shows the spectrum for the central core region within an angular radius of 0.°5; the middle and bottom panels present the spectra for regions A and B, as defined in (a), respectively. The vertical dashed lines indicate the Si II* and C IV lines, and the brightest H_2 fluorescence lines.

(A color version of this figure is available in the online journal.)

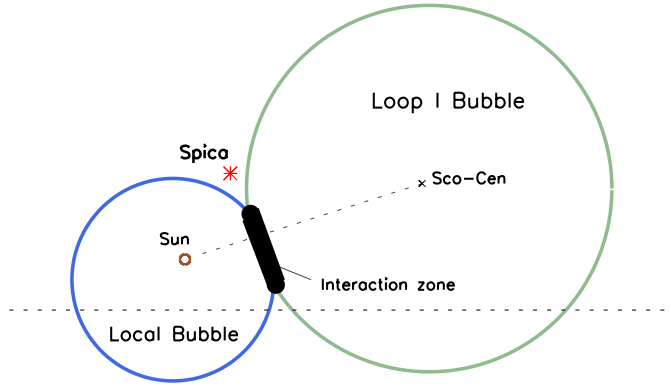

Figure 5. Schematic representation of the geometrical relation between the Local Bubble, Loop I, the interaction zone, and the central star Spica.

(A color version of this figure is available in the online journal.)

band. In the second model, they assumed an albedo of 0.4, and obtained a reasonable agreement with the observation by employing two dust layers, one at 2 pc from the star with 20% of the total dust assigned to it and the other at a distance of 30 pc from the star toward the Sun, with the remainder of the dust allocated to it.

In our study, we present an improved model that includes the dust-scattering effects of the interaction zone as well as the radiation field originating from the background stars near Spica, in order to study the extended region of the Spica Nebula. We employed a three-dimensional Monte Carlo radiative transfer code, in which photons are allowed to be multiply scattered (e.g., Seon & Witt 2012; Jo et al. 2012; Lim et al. 2013; Seon 2003). However, single dust scattering was dominant because the region is optically thin and the optical depth approaches ~1 in the interaction zone. The photon direction after each scattering was modeled by the Henyey–Greenstein phase function (Henyey & Greenstein 1941)

$$\phi(\theta) = \frac{a}{4\pi} \frac{(1-g^2)}{[1+g^2-2g\cos(\theta)]^{1.5}}, \quad (1)$$

where a and g are the albedo and the phase function asymmetry factor of dust scattering, respectively. The simulation code employed the peeling-off method (Yusef-Zadeh et al. 1984) for simulation efficiency; while each photon from radiation sources propagates through the dust medium and experiences multiple scatterings into random directions, the code stores the scattered fraction of the photon in the direction toward the Sun from each scattering, and these fractions are added up to give the final intensity. The parameters to be determined from the simulation are the albedo a, the asymmetry factor g, and the spatial distribution of dust. More detailed descriptions on the simulation technique can be found in Jo et al. (2012) and Lim et al. (2013).

The diffuse interstellar FUV emission is composed of three different components in addition to the dust-scattered starlight:

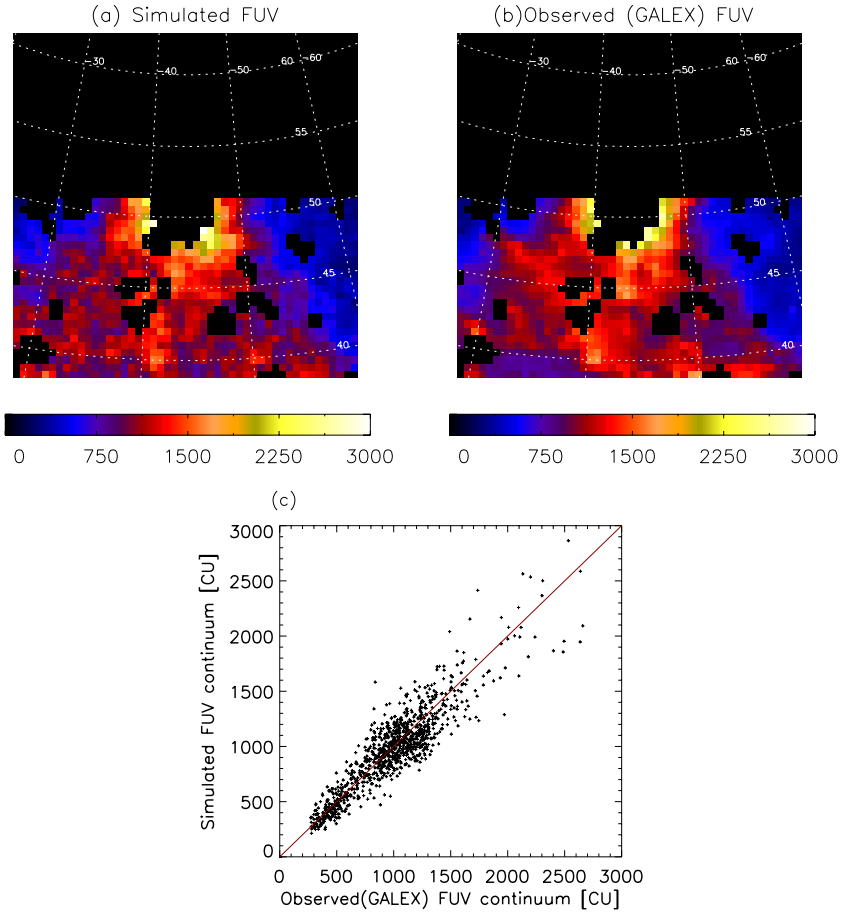

Figure 6. FUV continuum map of the southern region obtained from (a) the dust scattering simulation, and (b) the *GALEX* observation. A pixel-to-pixel correlation plot of the FUV intensity obtained from (a) and (b) is shown in (c).

(A color version of this figure is available in the online journal.)

ionic emission lines from hot gases of $10^{4.5}$–$10^{5.5}$ K, H_2 fluorescent emission lines originating from PDRs irradiated by interstellar UV photons, and two-photon continuum emission from the ionized gas of about 10^4 K. Therefore, in order to obtain only the dust-scattering component from the total observed FUV intensity, it is necessary to estimate various contributions to the observed FUV intensity. In addition, the isotropic background derived from the FUV intensity extrapolated to $N(\mathrm{H\,I}) = 0$ should be removed from the observed FUV intensity (Bowyer 1991; Henry 2002). In this study, we subtracted the minimum intensity of 200 CU as the contribution of the isotropic background. The two-photon emission was estimated using a simple formula of 60 CU per 1 R of Hα intensity (Reynolds 1990). However, this contribution is insignificant even in the Spica Nebula, with ~6% contribution to the total FUV intensity. The contribution of the two-photon continuum emission to the diffuse ionized gas or warm ionized medium outside of the Spica Nebula is also unimportant (see Seon et al. 2011a). The contribution of H_2 fluorescent emission is also negligible as it was estimated to be smaller than 10% even for the interaction zone.

The simulation domain consisted of 400 × 400 × 400 rectangular grids cells each with cell size of 1 pc. The central axis was chosen along the line of sight toward Spica, and the Sun was placed at the center of the front face of the simulation box. A total of 21,225 stars from the TD-1 and Hipparcos (Perryman et al. 1997) catalogs were disposed in the simulation box as radiation sources. A total of 10^8 photons were generated and assigned to the stars in proportion to their intrinsic luminosities. The spatial distribution of dust was obtained based on the Schlegel, Finkbeiner, and Davis (SFD) dust map (Schlegel et al. 1998). As the map is two-dimensional without the distance information along the line of sight, a dust slab with a thickness (t) was assumed to be located at a distance (d). The total dust column density along each sightline was uniformly distributed among the dust cells in the sightline. The optical depth at 1565 Å was derived from the $E(B-V)$ value of the SFD map with $R_V = 3.1$, the average value for the Milky Way. We assumed that the minimum $E(B-V)$ of 0.015 found in Figure 2 is not related to the dust around Spica and subtracted the value from the dust extinction map. Comparison between the simulation and the observation was made only for the region with an angular distance larger than 3°.5 from the central star as the *GALEX* data may not be reliable for the bright region close to the central star. The simulation parameters were varied as follows: the distance to the front face of the dust slab was varied from 50 to 90 pc in steps of 2 pc and the thickness from 10 pc to 50 pc in steps of 2 pc. We also varied the albedo (a) from 0.30 to 0.50 in steps of 0.02 and the asymmetry factor (g) from 0.40 to 0.60 in steps of 0.02. Each simulation was compared with the *GALEX* observation to obtain a set of best-fit parameters.

A Monte Carlo simulation of dust scattering does not constrain the scattering parameters effectively when only a single star is present, as discussed in Murthy & Henry (2011). In fact, such a simulation may produce many parameter sets that yield

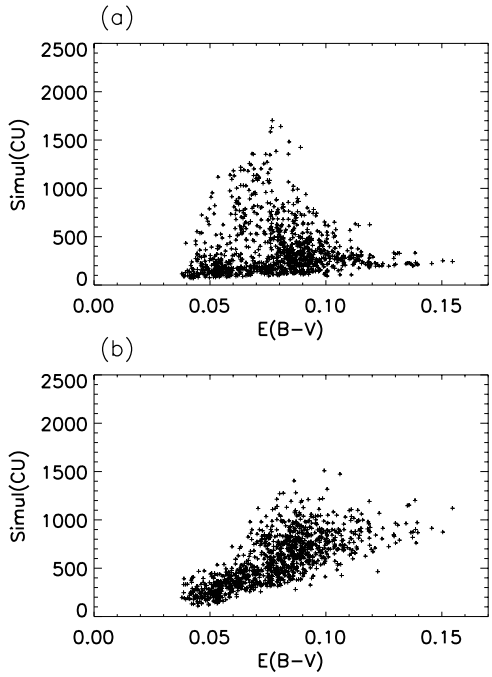

Figure 7. Simulated FUV intensity plotted against $E(B-V)$ for the southern region: (a) simulation with the central star only and (b) simulation with the background stars only.

similar FUV intensities. Hence, we first fitted the southern region to obtain the optical parameters of dust, excluding the northern region where Spica dominates the FUV intensity to reduce the effect caused by the bright central star. The dust parameters determined from the southern region will be adopted for the simulation of the northern region. The resulting best-fit parameters were $d = 70^{+4}_{-8}$ pc, $t = 40^{+8}_{-10}$ pc, $a = 0.38 \pm 0.06$, and $g = 0.46 \pm 0.06$. Figure 6 presents the best-fit simulation map together with the *GALEX* map and compares the calculated intensities with the observed value. The figure shows good agreement between the simulation and the observation. It should also be noted that Egger & Aschenbach (1995) suggested that the location of the interaction zone was ∼70 pc, which agrees with the present best-fit distance. Furthermore, the obtained optical parameters $a = 0.38$ and $g = 0.46$ accord well with the studies conducted for other objects (Jo et al. 2012; Lim et al. 2013), as well as with the theoretical predictions ($a = 0.4$–0.6 and $g = 0.55$–0.65) from the carbonaceous-silicate grains model (Weingartner & Draine 2001; Draine 2003). Hence, we use $a = 0.38$ and $g = 0.46$ in further discussions.

The contributions of the central star and background stars to the total FUV intensity are shown in Figures 7(a) and (b), respectively. Figure 7(a) shows that the contribution from the central star is most important for $E(B-V) \leqslant 0.06$, which is not surprising, as the distance from the central star increases with increasing $E(B-V)$. On the other hand, the background stars become more important than the central star for $E(B-V) > 0.06$. In fact, the structures of the interaction zone in the observed FUV map appear to match the simulation map obtained only with the background stars, which implies that the observed FUV intensity in the interaction zone is dominated by scattering of the photons of the background stars. It is also interesting to note that the simulated intensity is also limited by a maximum intensity of 1500 CU, due to the finiteness of the local stellar radiation field in the region.

We also performed radiative transfer simulations for the northern region, adopting the values of $a = 0.38$ and $g = 0.46$ and a single slab model. The distance to the front face and the thickness of the dust slab were 70 pc and 30 pc, respectively. That result implies that ∼33% of the dust is located in front of the central star and the remaining ∼67% behind the star. Figure 8 presents the resulting simulation map together with the *GALEX* observation and compares the simulation intensity with the *GALEX* intensity. As seen in the figure, the simulation and observation are in good agreement. With ∼33% of the dust located in front of the central star, the H I column density of the northern region, obtained using the net mean $E(B-V)$ value of ∼0.015 after subtracting the background of 0.015 and the relationship between N(H I) and $E(B-V)$ found in Figure 3, is estimated to be $\sim 3 \times 10^{19}$ cm^{-2}, which is similar to that ($\sim 10^{19}$ cm^{-2}) obtained for the shell boundary of the LB (Cox & Reynolds 1987; Lallement et al. 2003). Adopting a thickness of 10 pc, this gives a density of ∼0.9 cm^{-3}, which is consistent with those (∼0.6 cm^{-3} or 0.2–0.6 cm^{-3}) estimated for the H II region (Reynolds 1985; Park et al. 2010). While we used a single slab with a constant density and thickness, it is remarkable that the results accord well with those of other independent observations. We also tried two-slab models, representing the LB and Loop I boundaries, but the two slabs could not be separated effectively, perhaps because the density of the LB is similar to that of the ambient medium, and thus the present models are not able to discriminate the shell of the LB from the ambient medium.

Sallmen et al. (2008) analyzed the results of the FUV observations made by the *Far Ultraviolet Spectroscopic Explorer* satellite toward a single direction $(l, b) = (277°, 9°)$ at the boundary of the interaction zone. By comparing the O VI and C III intensities of two other neighboring directions across the boundary of the interaction zone, one just outside the interaction zone and the other inside the interaction zone, they were able to discriminate the contributions of Loop I from those of the LB by considering the fact that the interaction zone with a neutral hydrogen column density of N(H I) $\sim 4 \times 10^{20}$ cm^{-2} has a shadowing effect on the two FUV lines. The result shows that the O VI emission comes mostly from the interface on the Loop I side of the interaction zone while the C III emission is produced on the LB side of the interaction zone.

As the FIMS wavelength band includes the C IV doublet lines at ∼1550 Å, we conducted a similar study for regions A and B in Figure 4(a), which represent two distinct regions with different extinctions: region B, being part of the interaction zone, suffers more extinction for the emission originating from Loop I than region A does. The average $E(B-V)$ for region A is ∼0.015 after subtracting the background extinction of 0.015, which translates into an optical depth of 0.11 at 1565 Å, and the average value of $E(B-V)$ for region B is 0.075 after the background subtraction with a corresponding optical depth of 0.54 at 1565 Å. With the C IV intensities $I_A \sim 5800 \pm 1100$ LU and $I_B \sim 4300 \pm 1200$ LU determined in Section 2 for region A and B, respectively, we obtained the intensities $I_{\rm LB} \sim 1400 \pm 4000$ LU and $I_{\rm LI} \sim 4900 \pm 5400$ LU for the LB and Loop I, respectively. The large error ranges are caused by the exponential factors associated with extinctions when the observed uncertainties of I_A and I_B are used to derive $I_{\rm LB}$ and $I_{\rm LI}$. The result seems to imply that a larger portion of the C IV emission comes from Loop I than from the LB, although this is not conclusive because of the large error range.

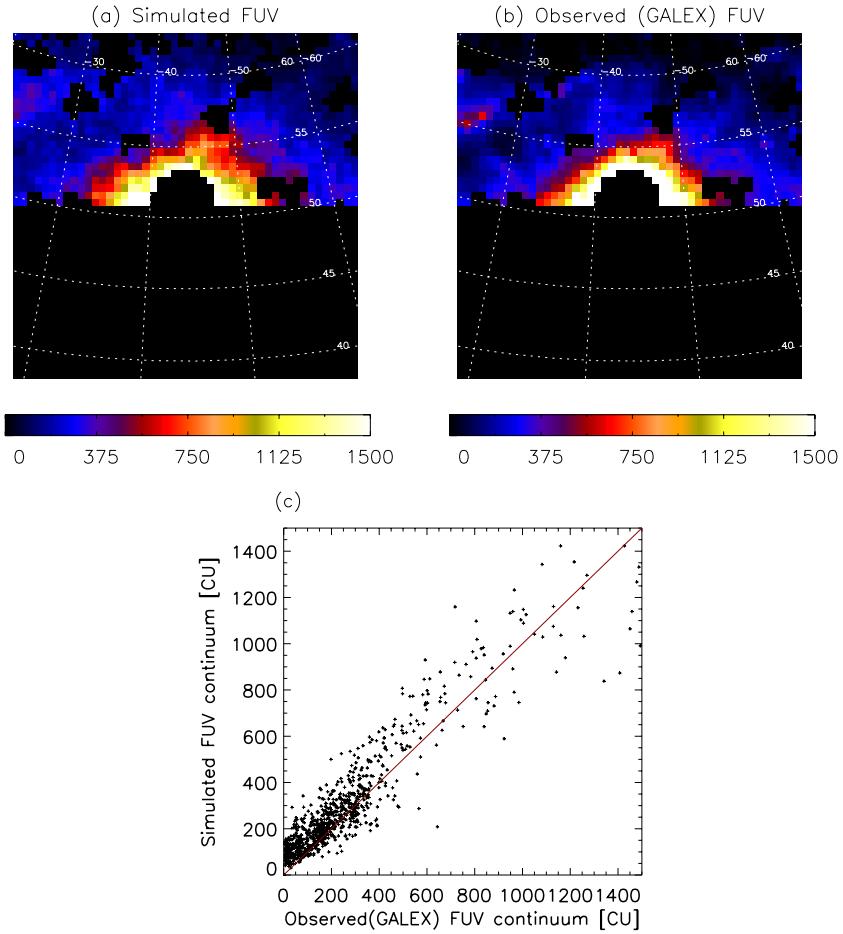

Figure 8. FUV continuum map of the northern region obtained from (a) the best-fit dust scattering simulation and (b) the *GALEX* observation. A pixel-to-pixel correlation plot of the FUV intensity obtained from (a) and (b) is shown in (c).
(A color version of this figure is available in the online journal.)

5. CONCLUSIONS

We have analyzed the data sets of the FUV observations performed by *GALEX* and FIMS, together with the maps constructed in other wavelengths, for the Spica Nebula and its neighborhood, which includes the interaction zone of Loop I and the LB. The following are the main findings of this study.

1. The diffuse FUV radiation observed in the northern region above Spica was mainly due to the dust scattering of starlight originating from Spica, while the diffuse FUV radiation in the southern region was attributed to scattering of photons originating from background stars by dust in the interaction zone.
2. The FUV intensity showed a general correlation with the dust color excess $E(B-V)$.
3. The ratio of neutral hydrogen to dust was about 7.0×10^{21} atoms cm^{-2}, which is slightly higher than previous studies estimated for diffuse ISM.
4. Diffuse C IV emission was observed throughout the whole region, including the interaction zone. By considering the shadowing effect in the interaction zone, we found that a larger portion of the C IV emission arises from the inner side of the shell boundary Loop I than in the LB.
5. Molecular hydrogen fluorescence lines were also observed in the interaction zone.
6. Based on the dust scattering simulation using a Monte Carlo radiative transfer code, we estimated the optical parameters of dust scattering as follows: $a = 0.38 \pm 0.06$ and $g = 0.46 \pm 0.06$, which are in agreement with previous radiative transfer studies as well as the theoretical dust grain models of the Milky Way.
7. We found that the interaction zone is located ~70 pc away from the Sun, with a thickness of ~40 pc, covering the southern neighborhood of the Spica Nebula. The central star Spica is likely to be located between the two shells of the LB and Loop I.

FIMS/SPEAR is a joint project of KAIST and KASI (Korea) and UC Berkeley (USA), funded by the Korea MOST and NASA grant NAG5-5355. This research was supported by the Basic Science Research Program (2010-0023909) and the National Space Laboratory Program (2008-2003226) through the National Research Foundation of Korea (NRF) funded by the Ministry of Education, Science, and Technology. The Wisconsin H-Alpha Mapper is funded by the National Science Foundation.

REFERENCES

Borkowski, K. J., Balbus, S. A., & Fristrom, C. C. 1990, ApJ, 355, 501
Bowyer, S. 1991, ARA&A, 29, 59
Breitschwerdt, D., Freyberg, M. J., & Egger, R. J. 2000, A&A, 361, 303
Burkhart, B., & Lazarian, A. 2012, ApJL, 755, L19
Burstein, D., & Heiles, C. 1978, ApJ, 225, 40
Corradi, W. J. B., Franco, G. A. P., & Knude, J. 2004, MNRAS, 347, 1065

Cox, D. P. 1998, in IAU Colloq. 166, The Local Bubble and Beyond, ed. D. Breitschwerdt, M. J. Freyberg, & J. Truemper (Lecture Notes in Physics, Vol. 506; New York: Springer), 121
Cox, D. P., & Reynolds, R. J. 1987, ARA&A, 25, 303
de Avillez, M. A., & Breitschwerdt, D. 2012, A&A, 539, L1
Diplas, A., & Savage, B. D. 1994a, ApJS, 93, 211
Diplas, A., & Savage, B. D. 1994b, ApJ, 427, 274
Draine, B. T. 2003, ApJ, 598, 1017
Edelstein, J., Korpela, E. J., Adolfo, J., et al. 2006a, ApJL, 644, L159
Edelstein, J., Min, K.-W., Han, W., et al. 2006b, ApJL, 644, L153
Egger, R., & Aschenbach, B. 1995, A&A, 294, L25
Ferlet, R., Vidal-Major, A., & Gry, C. 1985, ApJ, 298, 838
Finkbeiner, D. P. 2003, ApJS, 146, 407
Fruscione, A., Hawkins, I., Jelinsky, P., & Wiercigroch, A. 1994, ApJS, 94, 127
Górski, K. M., Hivon, E., Banday, A. J., et al. 2005, ApJ, 622, 759
Haffner, L. M., Reynolds, R. J., Tufte, S. L., et al. 2003, ApJS, 149, 405
Henry, R. C. 2002, ApJ, 570, 697
Henyey, L. G., & Greenstein, J. L. 1941, ApJ, 93, 70
Hurwitz, M. 1994, ApJ, 433, 149
Jo, Y.-S., Min, K.-W., Lim, T.-H., et al. 2012, ApJ, 756, 38
Jo, Y.-S., Min, K.-W., Seon, K.-I., et al. 2011, ApJ, 738, 91
Kalberla, P. M. W., Burton, W. B., Hartmann, D., et al. 2005, A&A, 440, 775
Kim, I.-J., Min, K.-W., Seon, K.-I., Han, W., & Edelstein, J. 2010a, ApJ, 709, 823
Kim, I.-J., Min, K.-W., Seon, K.-I., et al. 2007, ApJL, 665, L139
Kim, I.-J., Seon, K.-I., Min, K.-W., et al. 2010b, ApJ, 722, 388
Klessen, R. S. 2000, ApJ, 535, 869
Knapp, G. R., & Kerr, F. J. 1974, A&A, 35, 361
Knude, J. 1978, A&AS, 33, 347
Lallement, R., Welsh, B. Y., Vergely, J. L., Crifo, F., & Sfeir, D. 2003, A&A, 411, 447
Landini, M., & Monsignori Fossi, B. C. 1990, A&AS, 82, 229
Lee, D.-H., Yuk, I.-S., Jin, H., et al. 2006, ApJL, 644, L181
Lim, T.-H., Min, K.-W., & Seon, K.-I. 2013, ApJL, 765, L107
Markwardt, C. B. 2009, in ASP Conf. Ser. 411, Astronomical Data Analysis Software and Systems XVIII, ed. D. A. Bohlender, D. Durand, & P. Dowler (San Francisco, CA: ASP), 251
Morrissey, P., Conrow, T., Barlow, T. A., et al. 2007, ApJS, 173, 682
Murthy, J., & Henry, R. C. 2011, ApJ, 734, 13
Park, J.-W., Min, K.-W., Seon, K.-I., Han, W., & Edelstein, J. 2010, ApJ, 719, 1964
Park, J.-W., Min, K.-W., Seon, K.-I., et al. 2007, ApJL, 665, L39
Park, S.-J., Min, K.-W., Seon, K.-I., et al. 2009, ApJ, 700, 155
Park, S.-J., Min, K.-W., Seon, K.-I., et al. 2012, ApJ, 754, 10
Perryman, M. A. C., Lindegren, L., Kovalevsky, J., et al. 1997, A&A, 323, L49
Reis, W., & Corradi, W. J. B. 2008, A&A, 486, 471
Reynolds, R. J. 1985, AJ, 90, 92
Reynolds, R. J. 1990, in IAU Symp. 139, The Galactic and Extragalactic Background Radiation, ed. S. Bowyer & C. Leinert (Dordrecht: Kluwer), 157
Sallmen, S. M., Korpela, E. J., & Yamashita, H. 2008, ApJ, 681, 1310
Savage, B. D., & Mathis, J. S. 1979, ARA&A, 17, 73
Schlegel, D. J., Finkbeiner, D. P., & Davis, M. 1998, ApJ, 500, 525
Seon, K.-I. 2003, JKPS, 43, 565
Seon, K.-I. 2006, ApJL, 644, L175
Seon, K.-I. 2012, ApJL, 761, L17
Seon, K.-I. 2013, ApJ, 772, 57
Seon, K.-I., Edelstein, J., Korpela, E. J., et al. 2011a, ApJS, 196, 15
Seon, K.-I., & Witt, A. N. 2012, ApJ, 758, 109
Seon, K.-I., Witt, A. N., Kim, I.-J., et al. 2011b, ApJ, 743, 188
Shull, J. M., & van Steenberg, M. E. 1985, ApJ, 294, 599
Slavin, J. D. 1989, ApJ, 346, 718
Sofue, Y., Hamajima, K., & Fujimoto, M. 1974, PASJ, 26, 399
Sternberg, A. 1989, ApJ, 347, 863
Sujatha, N. V., Murthy, J., Suresh, R., Henry, R. C., & Bianchi, L. 2010, ApJ, 723, 1549
Thompson, G. I., Nandy, K., Jamar, C., et al. 1978, Catalogue of Stellar Ultraviolet Fluxes. A Compilation of Absolute Stellar Fluxes Measured by the Sky Survey Telescope (S2/68) Aboard the ESRO Satellite TD-1 (London: Science Research Council)
Vazquez-Semadeni, E. 1994, ApJ, 423, 681
Weingartner, J. C., & Draine, B. T. 2001, ApJ, 548, 296
Welsh, B. Y., Craig, N., Vedder, P., & Vallerga, J. V. 1994, ApJ, 437, 638
Welsh, B. Y., & Lallement, R. 2005, A&A, 436, 615
Welsh, B. Y., Lallement, R., Vergely, J., & Raimond, S. 2010, A&A, 510, 54
Willingale, R., Hands, A. D. P., Warwick, R. S., Snowden, S. L., & Burrows, D. N. 2003, MNRAS, 343, 995
Yoshioka, S., & Ikeuchi, S. 1990, ApJ, 360, 352
Yusef-Zadeh, F., Morris, M., & White, R. L. 1984, ApJ, 278, 186
Zagury, F., Jones, A., & Boulanger, F. 1998, in IAU Colloq. 166, The Local Bubble and Beyond, ed. D. Breitschwerdt, M. J. Freyberg, & J. Truemper (Lecture Notes in Physics, Vol. 506; Berlin: Springer), 385